DIFFERENTIATED HEATED LID DRIVEN CAVITY INTERACTING WITH TUBE
A Lattice Boltzmann Study

by

***Rachid BENNACER*[a,b*], *Marcelo REGGIO*[c], *Nicolas PELLERIN*[c], *and Xiaoyan MA*[a,b]**

[a] LMT /ENS-Cachan/CNRS/University of Paris Saclay, Cachan, France
[b] Tianjin Key Laboratory of Refrigeration Technology, Tianjin University of Commerce, Tianjin, China
[c] Polytechnic School of Montreal, Montreal, Canada

Original scientific paper
DOI:10.2298/TSCI160429238B

The multiple-relaxation time lattice-Boltzmann method is implemented to investigate combined natural and forced convection occurring in a 2-D square cavity. The top wall slides to the right at constant speed, while the other three remain stationary. The solution is performed for a left vertical wall at a constant temperature, which is higher than of the right wall. This yields a "co-operating" case, in which dynamic and buoyancy forces are added together. The enclosure is filled with air and contains a heat conducting circular cylinder, which is placed at various positions. The double distribution model used in lattice-Boltzmann methods has been adopted to simulate the hydrodynamic and thermal fields, with the D_2Q_9 and D_2Q_5 lattices selected to perform the corresponding computations. Simulations have been conducted over a wide range of Rayleigh and Reynolds numbers, and the features of dynamic and thermal fields are presented for the spectra of this mixed convection phenomenon. The flow and heat transfer characteristics of the cylinder position are described and analyzed in terms of the average Nusselt number. The computed results show the influence of the cylinder on the corresponding heat transfer in the enclosure. It has been found that the power (i.e. shear stress) needed to lid the upper surface will depend on the governing parameters.

Key words: *lattice-Boltzmann method, mixed convection, flow cylinder interaction*

Introduction

The flow problem in a 2-D lid driven cavity is a classical topic in scientific computing, which has been extensively studied using numerical methods for more than 40 years now. In a similar vein, numerous studies have treated the flow motion and heat transfer on a differentiated heated cavity. These basic tests cases have led to a huge number of publications which have explained the fundamental physics of different types of flows over a wide range of Reynolds and Rayleigh numbers. Moreover, the combination of both cavity flows, that is, mixed convection heat transfer, has also been widely analyzed, because this physical phenomenon takes place in a number of engineering devices and processes: heat exchangers, electronic part cooling, solar collectors, and glass coating, to name a few. The flow dragged by such moving wall impinges the vertical stationary wall, which directs the flow downward with sharp gradient is equivalent

* Corresponding author, e-mail: rachid.bennacer@ens-cachan.fr

to a wall jet. Secondary vortices form at the corner as the Reynolds number increases. Most of the studies on lid driven cavity consider steady state-condition. The brief state of the art for such mixed convection is available in [1]. In spite of this important body of applications, very few investigators have considered the case of mixed convection in cavities containing obstacles. Flow patterns are obviously modified by obstacles, but, most importantly, their presence has a direct impact on heat transfer and shear stress. The problem considered here involves a cavity which contains a circular cylinder. The top boundary of the cavity moves to the right, and the vertical walls are differentially heated. The cylinder, the diameter of which remains constant, is placed at various positions in the cavity. Because of the temperature difference applied along the vertical walls, buoyancy forces play a role and the flow becomes more complex than in a simple driven cavity. Depending on the side where the hot wall is located, left or right, a convective effect that works with or against the lid driven convection is obtained, respectively. The goal of our study is to characterize the heat transfer performance in the co-operating case, with respect to the cylinder position within the cavity, which will be assessed by means of the Nusselt number. The value of this parameter will ultimately provide an indication from which to infer the position of the cylinder in order to achieve improved heat transfer.

To address the issue of fluid flow and heat transfer, numerical studies have been performed during the past four decades or so, based on the solution of discrete forms of the Navier-Stokes (NS) equations, with techniques such as the finite volume, finite difference, or finite element methods. In contrast to this classical CFD methodology, a quite different understanding of *numerical fluid motion* has led to the development of a new method, called the lattice Boltzmann method (LBM) [1-8]. The LBM is a strategy with the distinctive feature of tackling complex flow problems across all scales: macro, micro, and nano.

The method can be derived in two different ways. It can be seen as a continuous version of a discrete micro-dynamic system that obeys simple rules, known as Cellular Automata (CA) [9-11]. Alternatively, the dynamics of the LBM can be obtained from the Boltzmann equation continuum, which concerns the motion of molecules in a gas and explains their behavior statistically at a continuum level.

The second approach, which establishes a direct link between the LBM and the Boltzmann equation from statistical mechanics, was introduced by Shan and He [6]. The works of Abe [12] and He and Luo [8] formally show that the LBM can be considered a specific discretization of Boltzmann equation without following the CA path.

The evolution of the particles is essentially split into two steps: streaming and collision. Key to the application of the LBM is the collision process. In order to simplify its treatment, a linearized collision operator [13] was introduced. A further enhancement was added by Higuera *et al.* [3], in which the link with the collision rules for the lattice gas was loosened, increasing its ability to handle more realistic Reynolds numbers. A crucial improvement was made with the introduction of a lattice Boltzmann version [4] of the Bhatnagar-Gross-Krook (BGK) model [14]. Owing to its exceptional simplicity, this single-relaxation time (SRT) model is the most popular variant of the collision operator today. In spite of its success, some shortcomings at the stability level have been pointed out by D'Humieres [15], and by Lallemand and Luo [16]. In this study, which is devoted to mixed-convection, we use the lattice Boltzmann multiple-relaxation time (MRT) methodology developed in a previous work [1] focusing on heat transfer performance on a rectangular cavity with different aspect ratios, A. Specifically, we extend the method to study the flow problem in a square lid driven cavity containing a circular cylinder, combined with the buoyancy generated by a horizontal temperature difference, that is, from vertical walls at different temperatures. The inclusion of such cylinder could modelizing the cross tube achieving the fluid distribution or, as in the present study, an obstacle modifying the flow structure and which could initiate unsteadiness.

Heat transfer is investigated for different Reynolds and Rayleigh numbers at various cylinder locations. The effect of the cylinder position on the heat transfer is assessed by means of the average Nusselt number.

The lattice Boltzmann numerical method

The LBM [17, 18], is based on a microscopic model that yields macroscopic fluid properties, such as density, velocity, and temperature. The so-called lattice-BGK (LBGK), a variant of the LBM introduced by Chen *et al*. [19], Koelman [20], and Qian *et al*. [4], can be seen as a discrete solution of the Boltzmann transport equation for particle distribution functions in a simplified phase space [8]. The corresponding physical space is usually represented by a Cartesian lattice.

In our work here, we have adopted the 2-D discretization, known as the D_2Q_9 lattice, for handling the flow dynamics, and the D_2Q_5 model for computing the temperature. With such discretization, sets of particles expressed by discrete distribution functions move on the lattices from cell to cell along nine (i = 1 to 9) or five (i = 1 to 5) directions, with constant molecular speeds, c_i, proportional to a constant lattice velocity $c = \delta x/\delta t$, where δx and δt are the lattice grid spacing and time step, respectively.

Let us now consider the fundamental distribution equation describing the evolution of the kinetic equation for the particle distribution function $f(x,c,t)$. This fundamental equation depends on the particle velocity, c, at location, x, and at time, t, and is given by:

$$\frac{\partial f}{\partial t} + c\nabla f = \Omega \tag{1}$$

The right-hand side of this equation indicates the diffusion process whereby the equilibrium distribution is rebuilt after the collision. The modeling of this term is crucial in the lattice Boltzmann approach, and there are various alternatives for treating it. We concentrate here on the D_2Q_9 lattice, in order to recall a few basic concepts.

For this lattice, the state of the fluid at location, x, and at time, t, is defined by means of nine (i = 0, 1,…, 8) distribution functions f_i following the discrete molecular speed c_i. Their evolution can thus be described by:

$$f_i(x + c_i, t+1) = f_i(x,t) + \Omega_i \tag{2}$$

In this expression, $c_i = 0$ for $i = 0$, takes the value 1 for (i = 1, 2, 3, 4), and corresponds to $2^{1/2}$ for (i = 5, 6, 7, 8). The mesh size is $\delta x = \delta y = 1$ and the time step $\delta t = 1$ in lattice units. For the D_2Q_9 lattice, the nine directions can be defined by:

$$c_i = \begin{cases} (0,0) & i = 0 \\ \cos[(i-1)\pi/2], \sin[(i-1)\pi/2](\delta x/\delta t), & 1 \le i \le 4 \\ \cos[(i-5)\pi/2 + \pi/4], \sin[(i-5)\pi/2 + \pi/4]\sqrt{2}(\delta x/\delta t), & 5 \le i \le 8 \end{cases} \tag{3}$$

The symbol Ω_i denotes the collision operator. The most popular approach for modeling it is what has been called the SRT LBGK model [4], given by:

$$\Omega_i = -\frac{1}{\tau}\left[f_i^{eq}(x,t) - f_i(x,t) \right]_i \tag{4}$$

where $f_i(x,t)$ and $f_i^{eq}(x,t)$ are the particle distribution function and the equilibrium particle distribution function of the ith discrete particle velocity c_i, respectively. The right-hand side rep-

resents the BGK collision, which accounts for the variation in the number of particles moving in each direction on the lattice due to microscopic inter-particle collisions [5]. These collisions are embedded in a SRT, τ, which is linked to the kinematic viscosity, ν, by:

$$\nu = \left(\tau - 1/2\right)\delta t\, c^2/3 \tag{5}$$

In spite of the simplicity of the SRT-BGK representation, a general alternative has been proposed to model the collision with the aim of improving the accuracy and stability of the method. This alternative is the MRT model [21].

The fundamental idea of MRT models is to transform the collision by projecting the discrete distribution functions into a so-called momentum space, and then relaxing these functions towards equilibrium with different relaxation times. The goal of this treatment is to improve the accuracy and stability of the numerical scheme.

When considering the MRT model, the collision operator can be expressed:

$$\Omega_i = -\sum_j \left(M^{-1}SM\right)_{ij}\left[f_i - f_i^{eq}\right] \tag{6}$$

where [M] indicates a transformation matrix which projects the discrete distribution functions f_i into a new set of variables m_i, leading to what is known as the moment space. This is achieved by applying $\boldsymbol{m} = M\boldsymbol{f}$ [22]. For the case of the D_2Q_9 lattice, $\boldsymbol{f} = [f_0, f_1, f_2, \ldots f_8]$, $\boldsymbol{m} = [m_0, m_1, m_2, \ldots m_8]$, and [M] is obviously a 9 × 9 matrix. According to the current D_2Q_9 lattice, the nine macroscopic moments are:

$$m = (\rho, j_x, j_y, e, \varepsilon, T_{xx}, T_{xy}, q_x, q_y) \tag{7}$$

All the elements of the moment vector have a physical meaning: fluid density $\rho = m_0$, the x and y momentum components j_x and j_y equal m_1 and m_2, respectively, a quantity $e = m_3$ is related to kinetic energy, a term $\varepsilon = m_4$ related to the square of the energy, quantities T_{xx} and T_{xy} corresponding to the diagonal and off-diagonal components of the stress tensor m_5 and m_6, respectively, and, finally, components q_x and q_y related to the energy fluxes m_7 and m_8, respectively.

The corresponding transform matrix [M] can be constructed via the Gram-Schmidt process [21, 23]. For the calculation of the temperature field, a second distribution function based on the internal energy, the evolution of which can also be followed with an MRT-LB modeling, is used. Specifically, the moment model is still applied, but with the first moment used to compute the density replaced by one suited for calculation of the temperature.

$$[\mathrm{M}] = \begin{bmatrix} 1 & 1 & 1 & 1 & 1 & 1 & 1 & 1 & 1 \\ 0 & 1 & 0 & -1 & 0 & 1 & -1 & -1 & 1 \\ 0 & 0 & 1 & 0 & -1 & 1 & 1 & -1 & -1 \\ -4 & -1 & -1 & -1 & -1 & 2 & 2 & 2 & 2 \\ 0 & 0 & -2 & 0 & 2 & 1 & 1 & -1 & -1 \\ 4 & -2 & -2 & -2 & -2 & 1 & 1 & 1 & 1 \\ 0 & 1 & -1 & 1 & -1 & 0 & 0 & 0 & 0 \\ 0 & 0 & 0 & 0 & 0 & 1 & -1 & 1 & -1 \\ 0 & -2 & 0 & 2 & 0 & 1 & -1 & -1 & 1 \end{bmatrix} \begin{matrix} \rho \\ j_x \\ j_y \\ e \\ \varepsilon \\ T_{xx} \\ T_{xy} \\ q_x \\ q_y \end{matrix}$$

The temperature is handled by the D_2Q_5 lattice topology, the discrete velocities, c_k, are:

$$c_k = \begin{cases} (0,0) & k = 0 \\ \cos[(k-1)\pi/2], \sin[(k-1)\pi/2]\delta x/\delta t, & 1 \le k \le 4 \end{cases} \tag{8}$$

$$g_k(x + c_k, t+1) = g_k(x,t) + \Omega_k \tag{9}$$

Like that of the density distribution function, the evolution of the discrete distribution functions g_k associated with the temperature can be written: in which the term Ω_k denotes the collision operator for the redistribution of the populations g_k on each site. Following the MRT method [22], this step is performed in the momentum space. For our D_2Q_5 lattice here, there are five moments m_k (instead of the nine for the D_2Q_9) related to the g_k distribution functions via $\boldsymbol{m} = M\boldsymbol{g}$ with [24]:

$$[\mathrm{M}] = \begin{bmatrix} 1 & 1 & 1 & 1 & 1 \\ 0 & 1 & 0 & -1 & 0 \\ 0 & 0 & 1 & 0 & -1 \\ -4 & 1 & 1 & 1 & 1 \\ 0 & 1 & -1 & 1 & -1 \end{bmatrix}$$

The first moment m_0 is conserved, and corresponds to the temperature, that is:

$$m_0 = \sum_{k=0}^{k=4} g_k \tag{10}$$

The non-conserved momenta are supposed to relax to an equilibrium m_k^{eq} state, as is the case for the density distribution function, that is:

$$m_k^{ac} = m_k^{bc} + s_k\left(m_k^{eq} - m_k^{bc}\right. \tag{11}$$

where s_k indicates the relaxation rate for each moment related to the evolution of the g_k populations. As for the hydrodynamic development, the s_k are not equal for each moment and need to satisfy the constraint $0 < s_k < 2$, in order for a numerically stable scheme to be achieved. As mentioned in [25], with the choice of $m_1^{eq} = 0$, $m_2^{eq} = 0$, $m_3^{eq} = 0$, and $m_4^{eq} = 0$, and using the Taylor expansion [24, 26], it is possible to find the diffusion equation up to order three in δt:

$$\frac{\partial T}{\partial t} - \frac{c^2\delta t}{10}(4+a)\left[\left(\frac{1}{s_1} - \frac{1}{2}\right)\frac{\partial^2 T}{\partial x^2} + \left(\frac{1}{s_2} - \frac{1}{2}\right)\frac{\partial^2 T}{\partial y^2}\right] + \theta(\delta t^3) \tag{12}$$

with $s_1 = s_2 = s$, $\delta x = \delta t = 1$, and $a = -2$, and, if for a given 2-D velocity field $\vec{\mathrm{u}}(u,v)$ it is considered that $m_1^{eq} = uT$, $m_2^{eq} = vT$, the lattice Boltzmann scheme yields the following classical diffusion equation:

$$\frac{\partial T}{\partial t} - \alpha\left(\frac{\partial^2 T}{\partial x^2} + \frac{\partial^2 T}{\partial y^2}\right) + \theta(\delta t^2) \tag{13}$$

in which

$$\alpha = \frac{\frac{1}{s} - \frac{1}{2}}{5} \tag{14}$$

Because of the temperature difference between the two vertical walls, a buoyancy $\vec{f} = \vec{g}\beta(T,x)$ acts in the y-direction (vertical), where $\vec{g}$ indicates the acceleration due to gravity and β the thermal expansion coefficient. Buoyancy corresponds to a body force which modifies the linear momentum conservation in the collisions. So, in general, for the f_x and f_y components of the body force, the formulas describing the moments m_1^{ac} and m_2^{ac} become:

$$m_1^{ac} = m_1^{bc} + f_x \tag{15-a}$$

$$m_2^{ac} = m_2^{bc} + f_y \tag{15-b}$$

Geometry and boundary conditions

The geometry, shown in fig. 1, consists of a 2-D square cavity with side length, L, containing a circular cylinder of radius $R/L = 0.1$. The top wall of the cavity is driven to the right at a constant speed, U_0, while all the other walls remain stationary. The vertical walls are maintained at different constant temperatures. The left wall is kept hot, at, T_H, while the right wall is kept cold, at, T_C. The top and bottom walls of the enclosure are kept in an adiabatic state. The cavity is filled with air (Pr = 0.71). The circular cylinder in the cavity conducts heat, so it is supposed to have the same thermal conductivity as the air, and its position will change horizontally at a constant height $H/L = 0.7$ measured from the bottom.

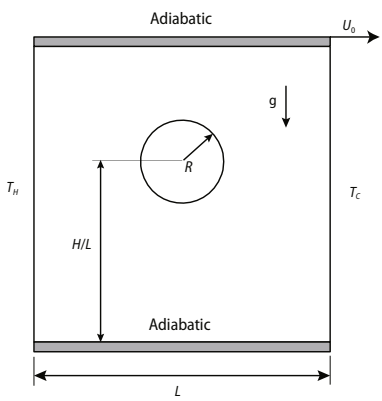

Figure 1. Geometry containing a circular cylinder and boundary conditions

The LBM is mostly applied on a regular Cartesian mesh, which is one of its practical advantages. Nevertheless, the accuracy in the handling of the curved boundaries can be improved, while maintaining Cartesian lattices over the entire domain. However, special treatment is clearly required to smooth out the irregularities caused by a Cartesian mesh on curved boundaries. One such treatment, which was introduced by Fillipova and Hanel [27] or by Mei *et al*. [28], can be seen more as a general bounce-back method. An alternative method was proposed by Guo *et al*. [29] for treating boundary conditions, including a combination of density, velocity, temperature, and their derivatives, or different, physically intuitive interpolation scheme introduced by Bouzidi *et al*. [30], based on the method of characteristics.

The left and right walls of the cavity are maintained at constant and different temperatures T_H and T_C, hot and cold, respectively. The upper and bottom surfaces are considered to be adiabatic. The inner circular cylinder is a heat conductor, and is assumed to have the same thermal conductivity as the fluid. The top boundary moves horizontally from left to right. The x-velocity component of the top surface is defined as U_0, while the y-velocity is obviously zero. Initially, the velocities at all nodes are set to zero, except for the upper-most nodes. The hydrodynamic boundary condition commonly applied on solid walls is the no-slip condition, which implies that the relative velocity of the fluid with respect to the wall vanishes. This is implemented in the LBM with the bounce-back rule, which establishes that all particles hitting the wall are reflected back in the direction of the source. Boundary conditions for the temperature are set between two consecutive nodes:

Left boundary: $\theta(0.5, y) = \theta_h = 0.5 \qquad (0.5 \le y \le N_y + 0.5)$

Right boundary: $\theta(N_x + 0.5, y) = \theta_c = -0.5 \qquad (0.5 \le y \le N_y + 0.5)$

Bottom boundary: $$\frac{\partial\theta}{\partial y}(x,0.5)=0 \qquad (0.5\le x\le N_x+0.5)$$

Top boundary: $$\frac{\partial\theta}{\partial y}(x,N_y+0.5)=0 \qquad (0.5\le x\le N_x+0.5)$$

where θ is the dimensionless temperature, and N_x and N_y are the lattice sites in the x and y directions, respectively. Noting that v_x and v_y are the velocity components along the x- and y-directions, respectively, the boundary conditions for the velocity at the top boundary can be written:

$$v_x(x,N_y+0.5)=U_0,\quad v_y(x,N_y+0.5)=0 \qquad (1/2\le x\le N_x+0.5)$$

All the other velocity components are zero on the remaining cavity boundaries, as well as on the cylinder periphery.

Results

In an earlier investigation, the current MRT model was validated for both natural convection and forced convection flows in a 2-D cavity. Then, a combined lid driven cavity investigation was carried out with co-operating and opposing thermal effects at different Rayleigh and Reynolds numbers [1, 31]. In the current study, a circular cylinder with a relative size R/L = 0.1, in which R indicates the radius of the cylinder and L the length of the side of the cavity, are introduced into the enclosure. Specifically, the cylinder is placed at five horizontal positions at a distance of $0.3L$ from the top. Its various locations are expected to show the impact on the flow characteristics and heat transfer strength (evaluated by the Nusselt number). As previously shown [1-31], natural or forced convection prevails, depending on the action of the Rayleigh or Reynolds numbers.

The current computational domain is composed of 200 × 200 lattice sites. This grid refinement was reached after a basic test for mesh independence. Calculations with successively refined grids were applied for a test with Re = 10^3 for pure forced convection, and with Ra = 10^6 for pure natural convection. When the error between the two finest meshes led to flow and temperature fields that varied by less than one order of magnitude, the last but one grid was chosen. Finally, the finest grid in the two situations was selected as the most suitable. The parameters taken into account to test mesh independence are standard for this kind of problem; namely, the average Nusselt number on the hot, Nu^+, and cold, Nu^-, vertical walls, respectively, and the maximum horizontal velocity component, u, evaluated at the midpoint of the vertical plane, $x = L/2$.

The results are presented and discussed in terms of dynamic and thermal fields. The evolution of the averaged heat transfer quantified by the Nusselt number is presented *vs.* the Rayleigh number, using the Reynolds number as a parameter. Results could also have been handled via Richardson's number, Ri = Ra/(PrRe^2), which translates the competition from natural to forced convection. In the study, the thermal conductivities of the solid cylinder and of the fluid have been set equal, and the calculations have been performed for the air as the working fluid, that is, for Pr = 0.7.

In an earlier work [31], pure natural convection tests (Re = 0) and pure lid driven cavity tests (Ra = 0) were performed using the current LB approach, and the results extensively compared and validated with classical benchmarks. This validation step is not repeated here. However, we did perform basic tests for mixed convection prior to the inclusion of the cylinder to provide a guide for assessing the relative changes as a result of combining buoyancy and shear forces. For purposes of research continuity, we have kept the same parameters as reported

in [31] to conduct this basic validation. Figure 2 illustrates the flow (stream function) and thermal (temperature) fields for a selected Re = 10^3 and for Ra = 10^{-3}, 10^3, 10^5, and 10^6.

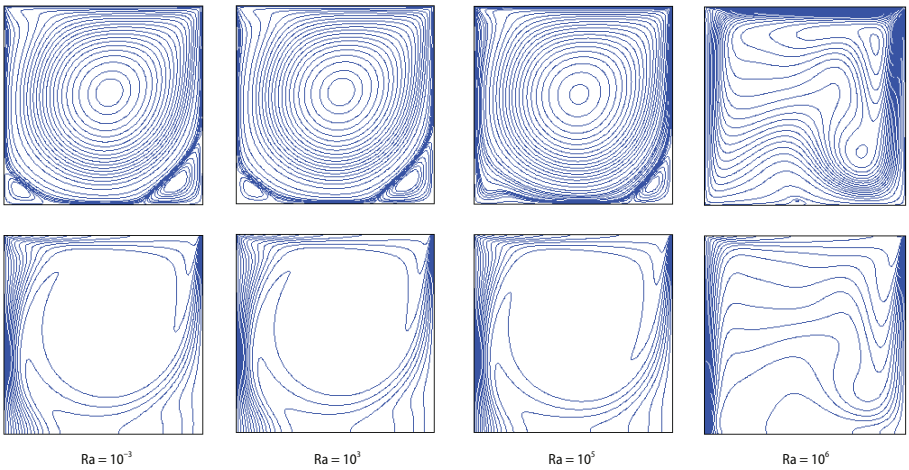

Figure 2. Streamlines and isotemperatures for various Rayleigh number values and Re = 10^3

Up to Ra = 10^5, the flow field is quite similar to a pure lid-driven cavity problem, while the temperature fields appear quite different from those achieved solely by a differentiated heated cavity, except for Ra = 10^6. This result simply indicates that, up to Ra = 10^5, forced convection prevails over natural convection and that the temperature field is modified by the dynamic structure. Note that the latter situation corresponds to the transition of Richardson number, Ri = Re/$Ra^{1/2}$, of order 1.

When the Rayleigh number increases, from 10^5 to 10^6, the impact of the buoyancy forces grows, and the leading role of the lid driven flow and the thermal flow changes. Natural convection now becomes dominant far from the lid surface for Ra = 10^6. This is clearly illustrated by the vertical stratification of isotherms, which resembles those found in a pure natural convection problem. This is verified by the flow field, which is now greatly affected by the strength of the buoyancy forces, and the flow in the bulk of the cavity is accelerated due to forced and natural effects combined. We note the effect on the thermal boundary layer of such a strong flow, which accelerates and moves from the heated wall to the cold one, inducing an irregular local heat transfer on the vertical walls. The flow in the bulk of the domain decreases, and separate boundary layers are observed on the different surfaces. Such localized flow with a relatively slower motion in the bulk of the domain is the reason for the mainly diffusive heat transfer responsible for the vertical stratification.

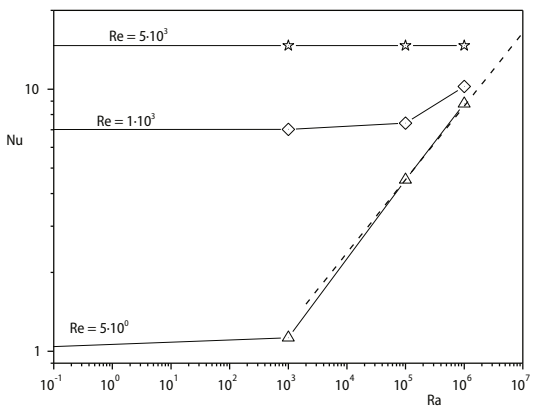

Figure 3. Evolution of the averaged Nusselt number (no cylinder enclosed)

For the (co-operating) case under study, fig. 3 shows the average Nusselt number as a function of the buoyancy (Ra) and driven (Re) forces. From the various plots, it can be clearly seen that heat transfer significantly

increases with both forced and natural convection. When the Rayleigh number increases, the results come closer to those obtained when pure natural convection takes place. In fact, for the situation of a developed boundary condition, the Nusselt number in natural convection takes the form $\mathrm{Nu} = 1/\delta \sim \mathrm{Ra}^{1/4}$, which is fitted as $\mathrm{Nu} = 0.277\mathrm{Ra}^{1/4}$.

For a higher Reynolds number ($5\cdot10^3$), the Nusselt number exhibits a constant behavior, *i. e.* it is independent of Rayleigh number, which illustrates the dominant effect of the lid driven condition. Rayleigh number values of 10^8 will be need to achieve a comparable effect (Ri ~1).

We now examine the flow and heat transfer characteristics when a circular cylinder is placed in the differentiated and heated lid driven cavity. The problem now has a new element, which is the cylinder's position. The horizontal position of the cylinder at a fixed height is analyzed as the governing parameter on the flow field, the temperature distribution, and the heat transfer. Computations are performed for five horizontal positions and one vertical location. The center of the cylinder is placed at a fixed vertical position of $y = 0.7L$, measured from the bottom, while the corresponding horizontal locations referring to the cavity center ($x = -0.5L$) are $x = -0.4L$, $-0.2L$, $0.0L$, $0.2L$, and $0.4L$. We note that, at positions $x = -0.4L$ and $x = 0.4L$, the flow passage is completely blocked between the cylinder and the left and right walls respectively. The following set of figures depicts the streamlines and isotherms computed for the five cylinder positions, complemented by the solution for the reference case, without the cylinder, at the left-most position. The tests were performed for $\mathrm{Ra} = 10^{-3}$, $\mathrm{Ra} = 10^3$, $\mathrm{Ra} = 10^5$, and $\mathrm{Ra} = 10^6$, and for $\mathrm{Re} = 1$, $\mathrm{Re} = 10^3$, and $\mathrm{Re} = 5\cdot10^3$. This means that the combined influence of Rayleigh and Reynolds numbers (natural or forced convection strength) on the flow and temperature fields, as well as the cylinder position, can be analyzed for an entire spectrum of cases.

For a viscous dominated flow, represented by Re = 1, the flow and temperature fields should correspond to those found for the situation of pure natural convection. In fact, as shown in figs. 4, and 5, the solution is completely governed by the buoyancy forces imposed by the temperature difference.

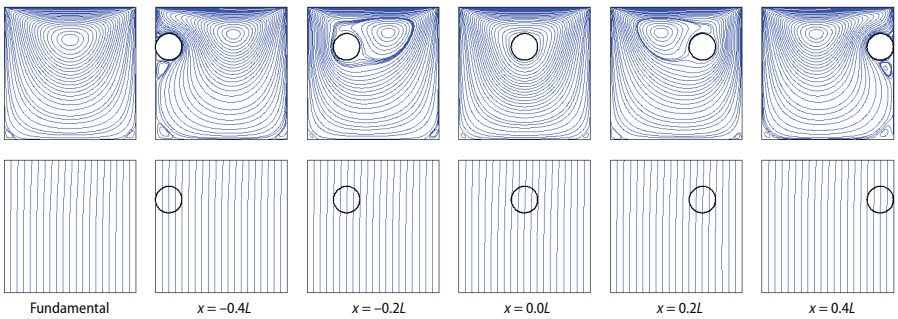

Figure 4. Streamlines (above) and isotherms (below) for Re = 1 and Ra = 10^{-3}

For the reference case, with no cylinder included, the resulting stream function and temperature fields match the well-known results established for the thermal cavity problem. The flow patterns show a clockwise rotating cell filling up the entire cavity with hydrodynamic boundary layers along the vertical walls and a motionless core region. The temperature field indicates the existence of thermal boundary layers along the vertical isothermal walls with a large temperature gradient in these regions. From figs. 2 and 4, we can see that including the cylinder affects the flow pattern for all Rayleigh numbers. Regarding the thermal field, its distribution is almost unaffected compared with the reference case, when the cylinder is located at the central positions $x = -0.2L$, $x = 0.0L$, and $x = 0.2L$. Nevertheless, the temperature field

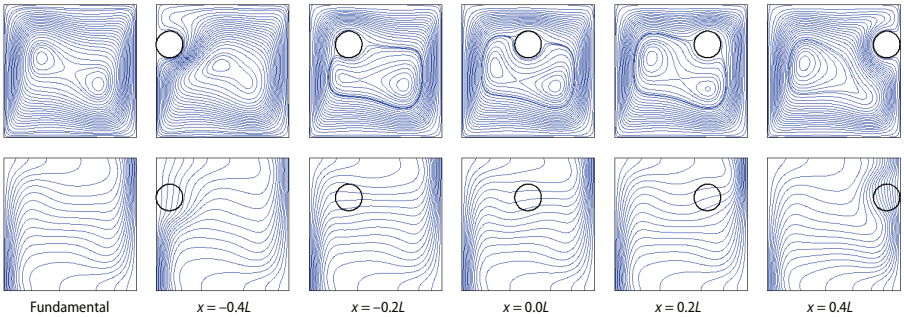

Figure 5. Streamlines (above) and isotherms (below) for Re = 1 and Ra = 10^5

is modified, mostly near the wall. Such modifications are not significant for weak Rayleigh number values, where thermal field is mainly diffusive, fig. 4. Looking at the recirculating flow below the tube (circle), we see that the modifications at high Rayleigh numbers, for positions $x = -0.4L$ and $x = 0.4L$, when the flow is blocked between the wall and the cylinder, are significant on the flow structure and on the thermal boundary layer. As the flow is mainly the consequence of the volumetric buoyancy forces, the previously underlined re-circulation in the vicinity of the cylinder disappears, fig. 5. This was expected, because the strength of the natural convection perturbs the dynamic boundary layer, even for such a low Reynolds number. The thermal field is relatively unaffected when the cylinder is outside the thermal boundary layer. We must also stress that such thermal stratification is unaffected, because the solid thermal conductivity is the same as that of the fluid.

For a higher Reynolds number of Re = 10^3, figs. 6-8 indicate that the flow is mainly governed by the lid driven force for Rayleigh numbers up to Ra = 10^5. With the exception of the position $x = 0.4L$, a large vortex rotating clockwise characterizes the phenomenon. When the buoyancy force increases further, the flow structure changes dramatically for all cylinder positions and the vortex center disappears to give rise to smaller re-circulation zones. Temperature gradient reversal is evident in the upper portion of the cavity, due to strong flow re-circulation at Ra = 10^6. In general, the isotherms are quite similar to those found in a pure thermal cavity test. For the central cylinder locations $x = -0.2L$, $x = 0.0L$, and $x = 0.2L$, the temperature distribution is almost unaffected by body inclusion, and is thermally identical to that of the fluid. It has been found that this phenomenon is almost the same for all Reynolds and Rayleigh numbers. At the left- and right-most cylinder positions, when the flow is completely blocked between the cylinder and the walls, the temperature and flow fields are more affected, mainly near the vertical walls that are kept at constant temperature.

The flow structure differs more from that of the reference case, with no immersed body, when the cylinder is at the right-most position than when is at the left-most location. It should be noted that, up to Ra = 10^5, the cylinder at the right-most position blocks the passage in such a way that part of the descending flow returns from right to left in the opposite direction to the lid motion. This leads to a vortex near the top that rotates clockwise, while a secondary vortex now appears that is rotating counterclockwise, *i. e.* a drag effect, fig. 6. The cylinder at the left-most position reduces the pressure effect and modifies the flow direction. This modification lessens the lid driven depth effect and allows the two corner re-circulating cells to collapse into one counter-rotating cell, fig. 6. As buoyancy increases, for Ra = 10^5, a thermal cell tends to settle and co-rotates with the lid driven one. In order to decrease the shear stress between the two cells at the cylinder vertical level, a tertiary vortex occurs, fig. 7. The upper vortex still rotates clockwise,

while a middle one rotates counterclockwise and a weaker vortex, at the cavity bottom, rotates clockwise. When buoyancy grows even stronger, characterized by Ra = 10^6, the tree vortex breaks-up, to yield a descending flow pattern that follows the cylinder boundary and continues further down, fig. 8. We can clearly see that the addition of the strength of buoyancy and lid driven forces produce a descending flow strong enough to overcome the obstruction caused by the cylinder. The local surface (pressure) forces become lower than the volumetric buoyancy forces, and a main cell is obtained comprising natural convection and lid driven effects.

For Re = $5 \cdot 10^3$, figs. 9 and 10, a dominating forced convection flow prevails almost everywhere. With such a high Reynolds number, the shear-induced fluid motion becomes dom-

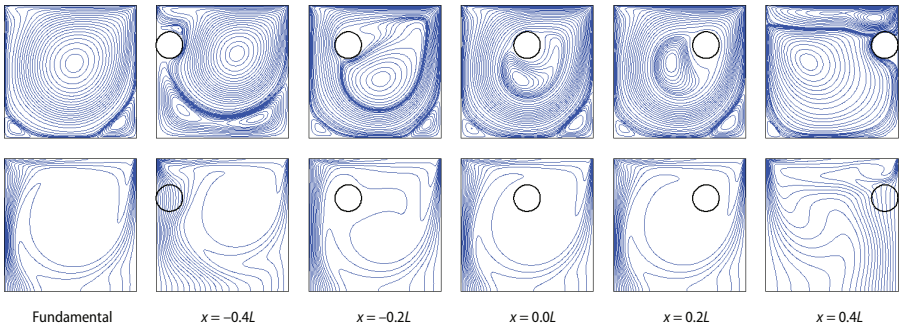

Figure 6. Streamlines (above) and isotherms (below) for Re = 10^3 and Ra = 10^{-3}

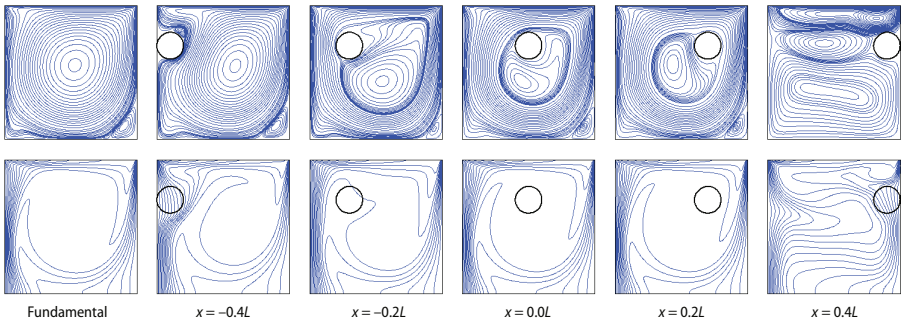

Figure 7. Streamlines (above) and isotherms (below) for Re = 10^3 and Ra = 10^5

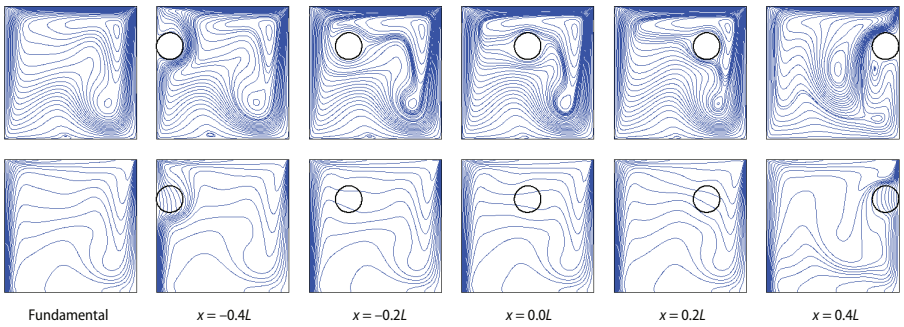

Figure 8. Streamlines (above) and isotherms (below) for Re = 10^3 and Ra = 10^6

inant and the re-circulation cell increases in size, occupying the central part of the cavity. As in the preceding cases, we can note that, for the non obstructed case, the dynamic structure does not change (it is the same as in the case of pure forced convection) with the Rayleigh number this time, even at a Rayleigh number of 10^6. Consequently, the thermal field appears almost undisturbed by the intensity of the Rayleigh number. As we found for lower Reynolds numbers, when the cylinder is located at $x = -0.2L$, $x = 0.0L$, and $x = 0.2L$, the core of the flow pattern is modified and secondary recirculation zones appear. Nevertheless, a large clockwise rotating flow prevails in all three cases. Also, the thermal field keeps the same qualitative structure as in the fundamental case. In fact, because the cylinder has the same thermal conductivity as the fluid, the isotherms are only slightly perturbed by the change in the flow pattern.

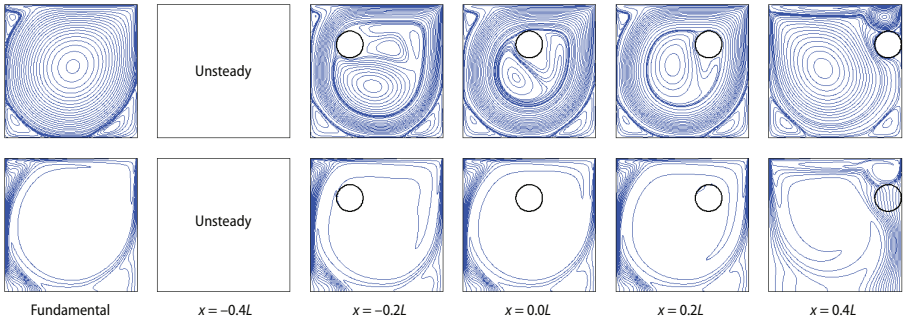

Figure 9. Streamlines (above) and isotherms (below) for Re = 5·10³ and Ra = 10³

For the left-most and right-most positions, a new phenomenon is observed. In fact, at the right-hand side, when the flow is blocked between the wall and the cylinder, the behavior is similar to that found for Re = 10^5. Specifically, a vortex rotating clockwise appears near the top, while up to Ra = 10^3 a secondary vortex is found rotating counterclockwise. For the stronger Rayleigh numbers of Ra = 10^5 and Ra = 10^6, there is a weaker tertiary vortex rotating clockwise, fig. 10. The situation dramatically changes when the flow is blocked at the left-most position. Now, independently of the buoyancy intensity, the lid driven forces produce a flow that yields unsteadiness behind the cylinder and there is no globally steady solution.

The cases for which Reynolds number based on the cavity length is higher than 10^3 will induce a maximum possible Re_c of 10^2, based on the cylinder's diameter. As the flow velocity intensity decreases from the level imposed by the moving boundary to rest on the dynamic boundary layer, we expect an average Re_c of the order of 50. We recall that the first unsteadiness

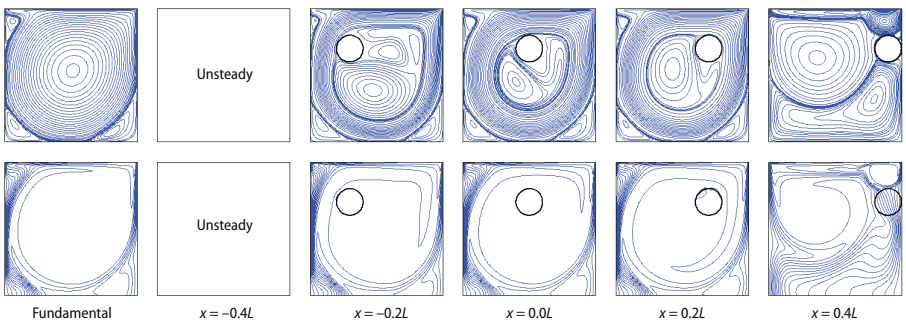

Figure 10. Streamlines (above) and isotherms (below) for Re = 5·10³ and Ra = 10⁵

of a flow around the cylinder is obtained for $Re_c > 41$, and that for such a Reynolds number the corresponding Strouhal number ($St = f D/V$) is approximately 0.2. We now turn to the core of this investigation, which is an analysis of the influence of the cylinder position, combined with the natural and forced convection intensity ratios, as represented by the Rayleigh and Reynolds numbers, respectively. The average Nusselt number for a steady, constant wall temperature is represented in figs. 11-13 *vs.* the Rayleigh number for Reynolds numbers of 1, 10^3, and $5 \cdot 10^3$ (in a mainly forced convection regime).

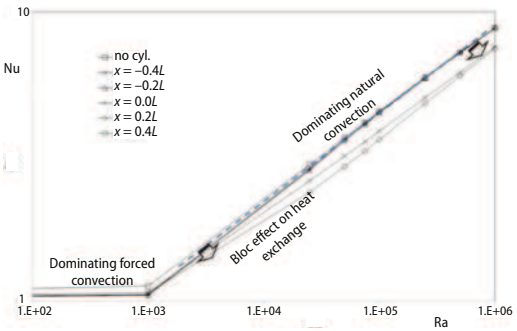

Figure 11. Evolution of Nusselt number at Re = 1 for the various cylinder positions

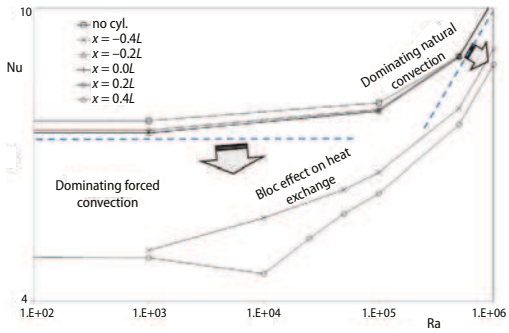

Figure 12. Evolution of Nusselt number at Re = 10^3 for the various cylinder positions

The set of curves in each figure shows what has already been indicated qualitatively by the streamlines and isothermal levels. Specifically, when the cylinder is sited at $x = -0.2L$, $x = 0.0L$, and $x = 0.2L$, the physics does not differ too much from the physics where there is no cylinder. On the contrary, when the cylinder blocks the flow between the left and right walls, the average Nusselt number falls by approximately 20% for the highest Rayleigh number from that of the reference cavity case with no immersed body. Comparison of these figures also indicates that the heat transfer increases with Reynolds number, due to the flow enhancement provided by the increasing inertia. The analysis clearly illustrates that heat transfer normally increases with the Rayleigh number when there is no cylinder included. This behavior corresponds to the classical mixed convection situation, where buoyancy forces became significant for the transition from convection to natural convection, as expressed by the Richardson number. The inclusion of a cylinder in the domain indicates that the overall heat transfer decreases in comparison to the reference case. It is important to note what happens to the local minimum heat transfer when the cylinder is close to the right-hand wall. The buoyancy forces induce a flow against the main cells resulting from the driven cavity and multicells are obtained, inducing several weak flow zones near the vertical surface.

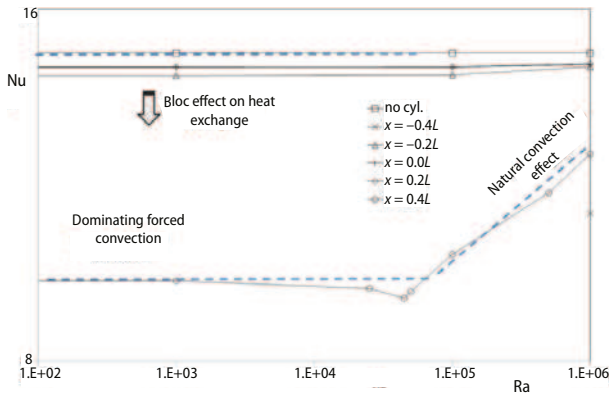

Figure 13. Evolution of Nusselt number at Re = $5 \cdot 10^3$ for the various cylinder positions

Conclusions

In this paper, we have applied a 2-D MRT thermal LBM to simulate flow and heat transfer in a square cavity filled with air and containing a circular cylinder. The cylinder is considered to have the same thermal conductivity as the air. After a basic grid convergence test, a discretization using 200 × 200 grid points has been used for all computations. The D_2Q_9 and D_2Q_5 lattices have been exploited to calculate the evolution of the velocity and temperature fields, respectively. The cylinder position was placed at a constant height at five horizontal positions. The top lid of the cavity slides at constant velocity and the vertical walls are at kept at different constant temperatures, while the horizontal walls are considered adiabatic. This combination of boundary conditions yields a mixed flow problem.

The study has been performed for an entire range of flows representing the combined effect of forced and natural convection, through a set of values for Ra = 10^{-3}, 10^3, 10^5, and 10^6 and for Re = 1, 10^3, and $5\cdot10^3$. From these twelve cases, it can be concluded that when the cylinder is located at the central positions of $x = -0.2L$, $x = 0.0L$, and $x = 0.2L$, heat transfer remains essentially the same as for an empty cavity. The impact is clear, though, at positions $x = -0.4L$ and $x = 0.4L$, when the flow passage is completely blocked between the cylinder and the walls. Although this could have been anticipated, because the cylinder position refashions the boundary layer along the walls, the study allowed us to quantify the impact of the inclusion on the average Nusselt number. Specifically, in the less negative situation, when natural convection dominates for Ra = 10^5, the Nusselt number drops, for all Reynolds numbers, to approximately 83% of the value found in the cavity with no cylinder. Some specific situations with local minimum heat transfer are noted, and the cylinder has no effect if it is placed away from the natural convection and lid driven boundary layers. The optimum situation will be a compromise, where heat transfer and lid power achieve a minimum, which will indicate the best efficiency exchange system. We stress the possibility of an unsteady oscillatory case, for which deeper investigation will be required. One interesting avenue could be the use of a temperature boundary condition or lid driven time modulation which would modify heat and shear stress. It would be possible to either amplify the unsteadiness (resonance) if the modulation is imposed at the same characteristic system frequencies or by damping the previous unsteadiness, if an adequate modulation phase delay is chosen.

Nomenclature

A – aspect ratio, (= H/L), [–]
c_i – discrete molecular speed, [ms^{-1}]
f – distribution function
f^{eq} – equilibrium distribution function
H – enclosure height, [m]
k – thermal conductivity, [Wm^{-1}K^{-1}]
L – enclosure width, [m]
Nu – Nusselt number, [–]
Pr – Prandtl number, (= ν/α), [–]
T – temperature, [K]
t – time, [s]
Ra – Rayleigh number, [= $(2T_0N^3a)/\nu k$], [–]
u – horizontal (x) velocity component, [ms^{-1}]
v – vertical (y) velocity component, [ms^{-1}]
X, Y – dimensionless co-ordinates, ($X = x/L$, $Y = y/L$), [–]
x, y – dimensional Cartesian co-ordinates, [m]

Greek symbols

α – thermal diffusivity, [m^{2}s^{-1}]
δt – time step, [–]
δx – lattice constant, [–]
ε – energy, [J]
ν – viscosity, [m^{2}s^{-1}]
Ω – collision operator, [–]
ρ – density, [kgm^{-3}]
τ – relaxation time, [s]

References

[1] Guo, Y., *et al*., Simulation of Mixed Convection in Slender Rectangular Cavity with Lattice Boltzmann Method, *International Journal of Numerical Methods for Heat & Fluid Flow*, *20* (2010), 1, pp. 130-148
[2] McNamara, G. R., Zanetti, G., Use of Boltzmann Equation to Simulate Lattice-Gas Automata. *Phys. Rev. L. 61* (1988), 20, pp. 2332-2335
[3] Higuera, F., *et al*., Lattice Gas Dynamics with Enhanced Collisions, *Europhys Lett., 9* (1989), 4, pp. 345-349
[4] Qian, Y., *et al*., Lattice BGK Models for Navier-Stokes Equation, *Europhys. Lett., 17* (1954), 3, pp. 479-484
[5] Bhatnagar, P., *et al*., A Model for Collision Processes in Gases: Small Amplitude Processes in Charged and Neutral One-Component Sys, *Phys. Rev., 94* (1954), 3, pp. 511-525
[6] Shan, X., He, X., Discretization of the Velocity Space in the Solution of the Boltzmann Equation. *Phys. Rev. Lett., 80* (1998), 1, pp. 65-68
[7] Abe, T., Derivation of the Lattice Boltzmann Method by Means of the Discrete Ordinate Method for the Boltzmann Equation, *J. Comp. Phys., 131* (1997), 1, pp. 241-246
[8] He, X., Luo, L.-S., Theory of the Lattice Boltzmann Method: From the Boltzmann Equation to the Lattice Boltzmann Equation, *Phys. Rev. E, 56* (1997), 6, pp. 6811-6817
[9] Von Neumann, J., Theory of Self-Reproducing Automata (Ed. Burks, A.), University of Illinois Press, Champaign, Ill., USA, 1966
[10] Frisch, U., *et al*., Lattice-Gas Automata for the Navier-Stokes Equation. *Phys. Rev. Letter, 56* (1986), 14, pp. 1505-1508
[11] d'Humieres, D., *et al*., Lattice Gas Models for 3D Hydrodynamics, *Europhy. Lett. 2* (1986), 4, pp. 291-297
[12] Abe, T., Derivation of the Lattice Boltzmann Method by Means of the Discrete Ordinate Method for the Boltzmann Equation, *J. Comp. Phys., 131* (1938), 1, pp. 241-246
[13] Higuera, F., Jimenez, J., Boltzmann Approach to Lattice Gas Simulations, *Europhys. Lett., 9* (1989), 7, pp. 663-668
[14] Bhatnagar, P., *et al*., A Model for Collision Processes in Gases: Small Amplitude Processes in Charged and Neutral One-Component System, *Phys. Rev., 94* (1954), 3, pp. 511-525
[15] D'Humieres, D., Generalized Lattice Boltzmann Equation, in Rarefied Gas Dynamics: Theory and Simulations in: *Progress in Astronautics and Aeronautics* (Eds. B. D. Shizgal, D. P., Weaver), AIAA, Washington D. C., 1992, Vol. 159, pp. 450-458
[16] Lallemand, P., Luo, L.-S., Theory of the Lattice Boltzmann Method: Dispersion, Dissipation, Isotropy, Galilean Invariance, and Stability, *Phys. Rev. E., 61* (2000), 6, pp. 6546-6562
[17] Succi, S.*, The Lattice Boltzmann Equation for Fluid Dynamics and Beyond*, Oxford University Press, Oxford, UK, 2001
[18] Wolf-Gladrow, D. A., *Lattice-Gas Cellular Automata and Lattice Boltzmann Models: an Introduction*, Springer-Verlag, Berlin, 2000
[19] Chen, S., *et al*., Lattice Boltzmann Model for Simulation of Magnetohydrodynamics, *Phys. Rev. Lett. 67* (1991), 27, pp. 3776-3779
[20] Koelman, J. M. V. A., A Simple Boltzmann Scheme for Navier-Stokes Fluid Flow, *Europhys. Lett. 15* (1991), 6, pp. 603-607
[21] Lallemand, P., Luo, L. S., Theory of the Lattice Boltzmann Method: Acoustic and Thermal Properties in Two and Three Dimensions, *Phys. Rev. E, 68* (2003), 3, pp. 036706.1-036706.25
[22] d'Humieres, D., Generalized Lattice Boltzmann Equations, in: *Rarefied Gas Dynamics: Theory and Simulations,* (Eds. B. Shizgal, D. P. Weaver), Prog. Astro. Aero., AIAA, Washington D. C., 1992, Vol. 159, pp. 450-458
[23] Lallemand, P., Luo L. S., Lattice Boltzmann Method for Moving Boundaries, *J. Comput. Phys., 184* (2003), 2, pp. 406-421
[24] Dubois, F., An Introduction to the Boltzmann Network Scheme, *ESAIM, 18* (2007), Sep., pp. 181-215
[25] Moussaoui, M. A., *et al*., A Computation of Flow and Heat Transfer Past Three Heated Cylinders in a Vee Vhape by a Double Distribution MRT Thermal Lattice Boltzmann Model, *International Journal of Thermal Sciences, 50* (2011), 8, pp. 1532-1542
[26] Dubois, F., Lallemand, P., Towards Higher Order Lattice Boltzmann Schemes, *J. Stat. Mech.* (2009), 6, pp. 1-40
[27] Filippova, O., Hanel, D., Grid Refinement for Lattice-BGK Models, *J. Comput. Phys. 147* (1998), 1, pp. 219-228

[28] Mei, R., *et al*., Force Evaluation in the Lattice Boltzmann Method Involving Curved Geometry, *Phys. Rev. E 65* (2002), 4, pp. 1-14
[29] Guo, Z. L., *et al*., An Extrapolation Method for Boundary Conditions in Lattice Boltzmann Method, *Phys. Fluids 14* (2002), 6, pp. 2007-2010
[30] Bouzidi, M., *et al*., Momentum Transfer of a Boltzmann Lattice Fluid with Boundaries, *Phys. Fluids 13* (2001), 11, pp. 3452-3459
[31] Ameziani, D. E., *et al*., Competition Between Lid-Driven and Natural Convection in Square Cavities Investigated with a Lattice Boltzmann Method, *Computational Thermal Sciences, 2* (2010), 3, pp. 269-282

Paper submitted: April 29, 2016
Paper revised: May 30, 2016
Paper accepted: June 29, 2016

© 2017 Society of Thermal Engineers of Serbia
Published by the Vinča Institute of Nuclear Sciences, Belgrade, Serbia.
This is an open access article distributed under the CC BY-NC-ND 4.0 terms and conditions